



HAL
open science

Response of East Asian Summer Precipitation to Intermediate SST Anomalies while El Niño Decays and Dependence on Type of Events

Na Wen, Laurent Li, Yongsheng Hao

► **To cite this version:**

Na Wen, Laurent Li, Yongsheng Hao. Response of East Asian Summer Precipitation to Intermediate SST Anomalies while El Niño Decays and Dependence on Type of Events. *Journal of Climate*, 2022, 35, pp.3845-3860. 10.1175/JCLI-D-21-0335.1 . insu-03726890

HAL Id: insu-03726890

<https://insu.hal.science/insu-03726890>

Submitted on 21 Feb 2024

HAL is a multi-disciplinary open access archive for the deposit and dissemination of scientific research documents, whether they are published or not. The documents may come from teaching and research institutions in France or abroad, or from public or private research centers.

L'archive ouverte pluridisciplinaire **HAL**, est destinée au dépôt et à la diffusion de documents scientifiques de niveau recherche, publiés ou non, émanant des établissements d'enseignement et de recherche français ou étrangers, des laboratoires publics ou privés.

Response of East Asian Summer Precipitation to Intermediate SST Anomalies while El Niño Decays and Dependence on Type of Events

NA WEN,^a LAURENT LI,^b AND YONGSHENG HAO^c

^a Center for Ocean–Atmosphere Interaction Research (COAIR) and College of Atmospheric Sciences, Nanjing University of Information Science and Technology, Nanjing, China

^b Laboratoire de Météorologie Dynamique, CNRS, Sorbonne Université, Ecole Normale Supérieure, Ecole Polytechnique, Paris, France

^c Network Center, Nanjing University of Information Science and Technology, Nanjing, China

(Manuscript received 30 April 2021, in final form 9 February 2022)

ABSTRACT: Impacts of El Niño on the following summer East Asian precipitation are dependent on its peak-time characteristics. Three types are identified and denoted as eastern Pacific (EP), mixed-type Pacific (MP), and central Pacific (CP) El Niño. For EP, excessive rainfall occurs in the Yangtze River valley, in relation to an anomalous anticyclone over the western tropical Pacific. For MP, a dipolar precipitation with anomalous wet conditions in northern China and dry conditions in east-central China is mainly due to an anomalous cyclone over Northeast Asia and a weak anticyclone over the Sea of Japan. For the case of CP El Niño, wetness along the Yangtze–Huaihe River valley and dryness in Southeast China are ascribed to an anomalous cyclone in Northeast China and a strong anticyclone over the western tropical Pacific. It is also revealed that the precipitation anomalies are fundamentally caused by different intermediate sea surface temperature (SST) anomalies from other basins while El Niño decays in the following summer. In the case of EP El Niño, the joint action from warm SST in the tropical Indian Ocean, the Niño-1.2 region, and the North Atlantic is responsible for the delayed effect of El Niño. For MP, the main delayed effect comes from warm SST in the northeast subtropical Pacific, developing La Niña, and cold SST in the southern tropical Atlantic. Finally, CP El Niño exerts its delayed influence through warm SST in the northern tropical Atlantic.

KEYWORDS: Atmosphere-ocean interaction; El Niño; Monsoons; Precipitation; Sea surface temperature

1. Introduction

El Niño is one of the most prominent sources of interannual variability of Earth's climate system. It exerts great influence on global climate, not only in its mature phase in boreal winter, but also in its decaying phase in the following spring and summer (Rasmusson and Carpenter 1982; Ropelewski and Halpert 1987). As a regional manifestation, East Asia is significantly impacted by El Niño, but shows complex relations and physical mechanisms. Huang and Wu (1989) found that in the following summer after El Niño peaks in the preceding winter, the Yangtze River and Huaihe valleys show dry conditions, sandwiched by anomalous wetness in North China and South China. This result is consistent with that of Chen (2002) and Wu et al. (2003). However, many other studies (Zhang et al. 1999; Chang et al. 2000; Wang and Zhang 2002; Wu et al. 2009) revealed wet conditions in the middle and lower reaches of the Yangtze River in the following summer of El Niño, such as the case of 1997/98.

Beyond the simple phenomenological description, there are also studies focusing on any underlying mechanisms of the El Niño delayed effect on East Asian climate. In principle, the atmospheric response to an SST anomaly should be almost simultaneous, because of its rapid adjustment within the time of

a few weeks (e.g., Hoskins and Karoly 1981; Peng and Whitaker 1999; Li and Conil 2003). Since El Niño SST anomalies almost disappear in the following summer, an intuitive thinking is to search intermediate players such as SST anomalies in other oceanic basins, which could relay the winter El Niño effect. But there is no consensus in the climate research community on these intermediate players and on how they operate (Xie et al. 2016; Li et al. 2017). Wang and Zhang (2002) and Wang et al. (2003) suggested that the local air–sea interaction between the cold SST anomaly and the westward propagating anticyclone in the western North Pacific sustains the Philippine Sea anticyclone (PSAC) into the following summer and therefore sustains the El Niño effect beyond its peak in precedent winter. Yang et al. (2007) and Xie et al. (2009) argued that it is the basinwide warming over the tropical Indian Ocean that prolongs the El Niño influence into the following summer. The winter-peaked El Niño-induced warming over the tropical Indian Ocean persists into the following summer and then feeds back to the atmosphere, ultimately resulting in the PSAC and precipitation anomalies over East Asia. In addition, a few scientists (Rong et al. 2010; Hong et al. 2014; Chen et al. 2016; Feng and Chen 2021) proposed a possible role of the tropical Atlantic in bridging the winter El Niño effect on the East Asian climate in the following summer.

Another prominent feature of El Niño is its diversity and irregularity. Different types of El Niño exist and exert influences on global climate with subtle differences (Wang and Hendon 2007; Weng et al. 2009; Taschetto and England 2009; Feng et al. 2011; Karori et al. 2013). Based on the spatial distribution characteristics of anomalous SST in the tropical Pacific, El Niño can be

Supplemental information related to this paper is available at the Journals Online website: <https://doi.org/10.1175/JCLI-D-21-0335.s1>.

Corresponding author: Na Wen, wenna@nuist.edu.cn

generally regrouped into two types (Ashok et al. 2007; Kao and Yu 2009; Kug et al. 2009): one is the eastern Pacific (EP) El Niño (so-called conventional El Niño), which is characterized by a major warming in the eastern Pacific; the other is the central Pacific (CP) El Niño (also called warm pool El Niño or El Niño Modoki), with maximum SST anomalies located in the central equatorial Pacific. Feng et al. (2011) found that the conventional El Niño induces precipitation anomalies over East Asia in the following summer in the form of a tripolar pattern with anomalous wetness over northern and southern China sandwiching anomalous dryness over the Yangtze–Huaihe River valley. El Niño Modoki, however, induces an almost out-of-phase response with positive precipitation anomalies over the Huanghuai River valley and negative ones over southern China. However, Yuan and Yang (2012) and Li et al. (2014) found that EP El Niño implies abundant precipitation over the Yangtze River valley and deficient rainfall over southern China, but CP El Niño shows insignificant impact on East Asian precipitation in the following summer.

These controversies of El Niño impacts on East Asian precipitation in the following summer prompt us to reconsider their relationships, mainly in terms of event classification. While studying the impact of El Niño on autumn precipitation over East Asia, Wang and Wang (2013) reclassified El Niño Modoki as types I and II to enhance the signal-to-noise ratio. Wen et al. (2020) also pointed out that it is necessary to separate the mixed-type (MP, for mixed Pacific) El Niño from the EP and CP El Niño in the developing summer, due to its distinguishing impact on the simultaneous precipitation over East Asia. Feng et al. (2020) further differentiated the El Niño Modoki cases to evaluate the relative contribution of warm SST over the tropical North Atlantic and cold SST over the central-eastern Pacific to the anomalous anticyclone over the western North Pacific in their decaying summer. These studies indicate that an appropriate classification of El Niño is essential to accurately assess their impacts on East Asian climate.

Another important issue is the identification of precise intermediate players in sustaining the delayed effects. Previous studies (He et al. 2015; Xie et al. 2016; Zhang et al. 2017; Li et al. 2017; Yu et al. 2021) indicated the potential effects of other regions to relay the winter El Niño impact into the following summer, as the tropical Indian Ocean does. Based on the general El Niño index (Niño-3.4), Wen and Hao (2021) revealed that besides the tropical Indian Ocean, SST anomalies over the western tropical North Pacific, the tropical North Atlantic, and the eastern-central subtropical South and North Pacific could be the potential intermediary in relaying the winter El Niño effect. So a legitimate question that arises is the following: Are the intermediate players different for different types of El Niño? If the answer is the anticipated affirmative, which other oceanic basins are the key regions in sustaining delayed effects of El Niño?

In this study, we will address these questions by carefully diagnosing relevant data from observations and reanalyses. The paper is arranged as follows. Data and methods are introduced in section 2. The impacts of different types of

El Niño on East Asian precipitation in the following summer and their associated regional circulation anomaly are documented in section 3. SST anomalies in key regions playing an important role are identified in section 4. Section 4 also presents physical mechanisms for those SST anomalies to exert their impact. These results are further confirmed by modeling experiments. A summary and discussion are given in section 5.

2. Data and methods

Precipitation is from the Chinese Meteorological Data Center, China Meteorological Administration compiling observations of 160 meteorological stations for the period of 1958–2016. The domain of our investigation is East China (east of 100°E), including 140 quite evenly distributed stations. To reduce noise, the raw dataset is reconstructed with the first 27 leading modes of empirical orthogonal function (EOF), retaining about 70% of the total variance. The precipitation variability is represented by the percentage of rainfall anomaly, defined as the ratio of the precipitation anomaly to its seasonal climatological mean at each station. Monthly sea surface temperature (SST) and atmospheric variables are from the National Centers for Environmental Prediction–National Center for Atmospheric Research (NCEP–NCAR) reanalysis data (Kalnay et al. 1996), with grid on $2.5^\circ \times 2.5^\circ$ for the same period. Anomalies of all variables are deviations from their mean seasonal cycle, and long-term trends are removed through a third-order polynomial filter. We should mention that main conclusions presented in the paper are unchanged, regardless of data sources. Our results remain robust with the Hadley Center Global Sea Ice and Sea Surface Temperature (HadISST; Rayner et al. 2003) SST and the European Center for Medium-Range Weather Forecasts (ECMWF) reanalysis (ERA-40; Dee et al. 2011).

Our classification of El Niño follows Kug et al. (2009) using the criterion of geographic location of the maximum SST anomalies in the equatorial Pacific. Besides EP and CP, MP El Niño is now listed as a separate type. In fact, this type of El Niño is often observed with maximum SST anomalies situated in the Niño-3.4 region. Prior to classification, El Niño events are determined first according to criteria defined and used at the Climate Prediction Center (CPC) of the U.S. National Oceanic and Atmospheric Administration. That is, the 3-month running mean SST anomalies in the Niño-3.4 region (5°S – 5°N , 120° – 170°W) must exceed the threshold of $\pm 0.5^\circ\text{C}$ for a minimum of five consecutive overlapping seasons. From 1958 to 2016, we selected 17 El Niño events. They are further classified into three types following the location of their maximal SST anomalies in boreal winter [the 3-month mean of December, January, and February (DJF)]: 5°S – 5°N , 150° – 90°W (the Niño-3 region; EP), 5°S – 5°N , 170° – 120°W (the Niño-3.4 region; MP), and 5°S – 5°N , 170°E – 150°W (roughly the Niño-4 region; CP), as indicated by the blue boxes in Fig. 1. Actually, there are five EP, five MP, and seven CP El Niño cases identified, as listed in Table 1. A few cases of El Niño are excluded from our analysis, because of competing centers of SST anomalies

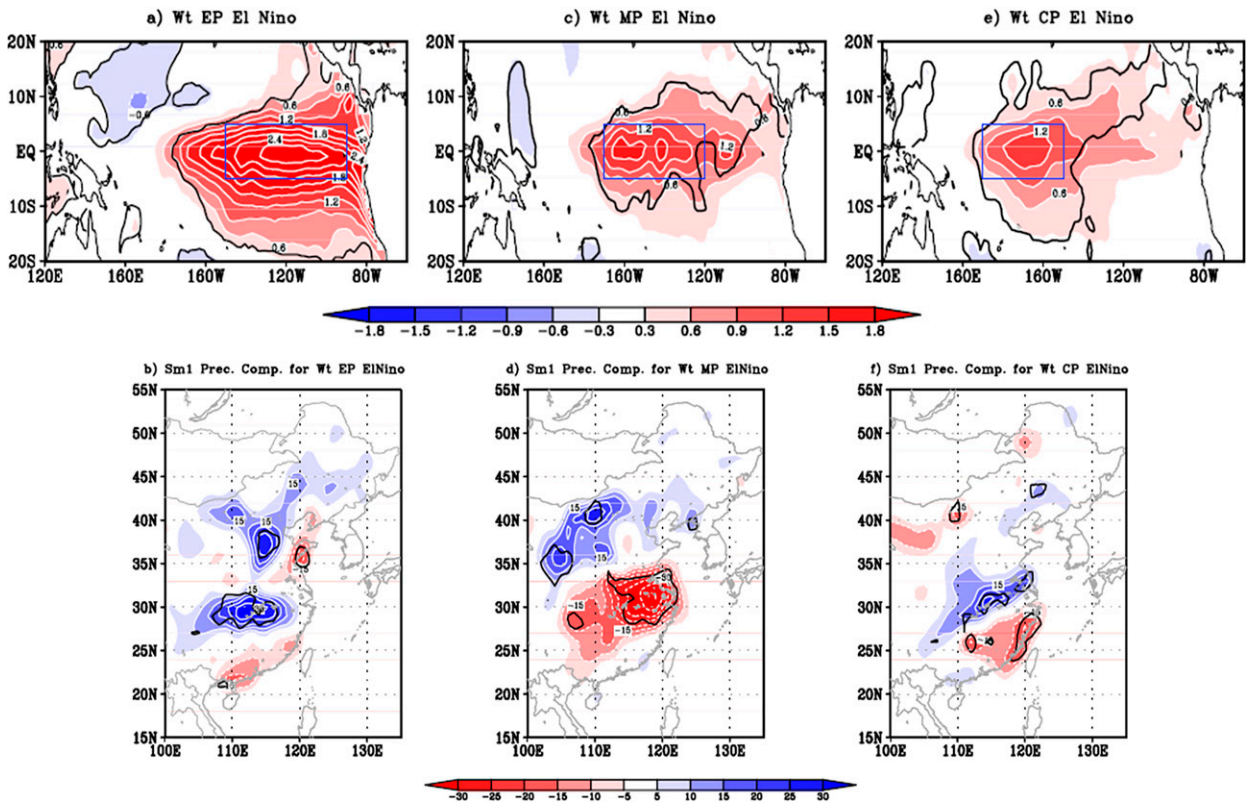


FIG. 1. (top) Composite sea surface temperature (SST; in K; contour interval: 0.3 K; peak winter DJF) and (bottom) East Asian precipitation anomalies (in %; contour interval: 5%; decaying summer JJA) for the three types of El Niño: (left) EP, (center) MP, and (right) CP. Blue boxes in the top panels show the geographic locations used to regroup El Niño events into three types: 5°S–5°N, 150°–90°W; 5°S–5°N, 170°–120°W; and 5°S–5°N, 170°E–150°W. The thick black contour denotes the 90% confidence level for precipitation, but 95% confidence level for SST anomalies.

along the equatorial Pacific or maximum SST anomalies out of the equatorial Pacific.

The composite methodology is then used with the statistical significance examined by the two-tailed Student’s *t* test. We also use the equilibrium feedback assessment (EFA) method as an independent evaluation to assess impacts of anomalous SST on the atmosphere. EFA is able to robustly assess atmospheric response to underlying simultaneous SST forcing, even with a strong presence of atmospheric internal variability. Details of the EFA methodology can be found in Frankignoul et al. (1998), Liu et al. (2008), and Wen et al.

(2010, 2015). Here we describe it briefly. Given the atmospheric variability $A(t)$ and SST variability $T(t)$ on monthly time scale, the atmospheric variability can be decomposed into the SST forcing term $b \times T(t)$ and the atmospheric internal variability $N(t)$, such that

$$A(t) = b \times T(t) + N(t), \tag{2.1}$$

where b indicates the SST feedback coefficient. Due to the fact that leading ocean cannot be affected by lagged atmosphere ($\langle N(t), T(t - \tau) \rangle \geq 0$), the feedback coefficient b can be derived as

TABLE 1. Pattern congruence coefficient (Prec. corr.) of the East Asian precipitation anomaly between the composite and each individual member for different types of winter El Niño. The boldface italic value denotes the 90% confidence level. Asterisks (*) indicate the year in which the intermediate SST anomalies appear for each type of El Niño.

EP	El Niño year	1973	1977	1983	1998	2016	
	Prec. corr.	<i>0.36</i>	<i>0.58*</i>	<i>0.34*</i>	<i>0.55*</i>	<i>0.69*</i>	
MP	El Niño year	1958	1964	1966	1978	1992	
	Prec. corr.	<i>0.54*</i>	<i>0.58*</i>	<i>0.59*</i>	<i>0.85*</i>	<i>0.45*</i>	
CP	El Niño year	1969	1988	1991	1995	2003	2010
	Prec. corr.	<i>0.47*</i>	0.18*	<i>0.69</i>	0.09*	<i>0.43*</i>	<i>0.38*</i>

$$b(\tau) = \frac{\langle A(t), T(t - \tau) \rangle}{\langle T(t), T(t - \tau) \rangle}, \quad (2.2)$$

where $\langle X, Y \rangle$ denotes the covariance of two variables, and τ is SST leading time, here taken as one month. For example, for the summer feedback coefficient b , it is calculated as the ratio of the covariance of the atmosphere in June–August (JJA) with the leading SST in May–July (MJJ) to the autocovariance of SST in JJA and MJJ. The significance of b is checked by the Monte Carlo method, in which the year of the atmospheric variable is scrambled randomly 1000 times, while the order of the months within a year is retained.

3. Impacts from different types of El Niño on East Asian climate

In Figs. 1a, 1c, and 1e, we can see significant differences among the three types of El Niño in terms of geographic location of their anomalous SST center. In EP El Niño (Fig. 1a), broad SST anomalies along the coast of South America gradually shrink westward to the central equatorial Pacific, with maximum anomalies falling into the Niño-3 region (as indicated by the blue box in Fig. 1a). This pattern resembles the canonical structure of conventional El Niño. For MP El Niño (Fig. 1c), the distribution of SST anomalies along the equatorial Pacific is quite different from that of EP El Niño. The main body of the ellipsoidal SST anomaly is away from the coast of South America by approximately 30 degrees of longitude, with the anomaly center over the Niño-3.4 region. In contrast to EP and MP El Niño, the distribution of SST anomalies for CP El Niño (Fig. 1e) is relatively small, mainly confined to the central tropical Pacific (east of Niño-4 region). According to the position where the maximum SST anomaly occurs, the three types of El Niño could be well separated. Among the three types, the amplitude of EP El Niño is the largest with the anomaly center around 2.1°C (the blue box in Fig. 1a). Super El Niño events are generally classified into this group, as listed in Table 1. The SST anomaly of MP El Niño is moderate with amplitude around 1.2°C in the blue box in Fig. 1c. And the weakest is CP El Niño with magnitude 1.0°C in the blue box in Fig. 1e. Since late 1980s, many CP El Niño cases are observed (Table 1), which is consistent with previous studies of Yeh et al. (2009) and Pascolini-Campbell et al. (2014).

a. Precipitation

Corresponding to the three types of El Niño, Fig. 1 shows distinct precipitation responses over East Asia in the following summer. For EP El Niño (Fig. 1b), the significant feature is the excessive precipitation along the Yangtze River valley with maximum amplitude up to 30%. This is consistent with previous studies (Zhang et al. 1999; Wang and Zhang 2002; Wu et al. 2009) showing that the Yangtze River generally experiences flooding in the following summer of super El Niño. There are also some insignificant precipitation anomalies with slight dryness in southern China and wetness in northern China. MP El Niño has a pronounced dipolar pattern with dry conditions in the Yangtze–Huanghuai River valley and wet conditions in

northern China (Fig. 1d). The amplitude is around 20%–35% of the summer mean precipitation, which passes the 90% confidence level. The precipitation anomalies are almost opposite to those of EP El Niño over the Yangtze–Huaihe River, but they are partly coincident with the results of Huang and Wu (1989) and Wu et al. (2003). In CP El Niño, the robust precipitation anomaly (Fig. 1f) presents a dipolar pattern in South China with abundant rainfall slightly tilting along the Yangtze–Huaihe River valley and deficient rainfall in southeast China. The anomalous amplitude is around 10%–20% with maximum values in the middle reaches of the Yangtze River.

To check the signal-to-noise ratio for each type of El Niño, the spatial pattern (over East China, east of 100°E) congruence coefficient of precipitation anomalies between the ensemble mean and individual members is calculated. As shown in Table 1, most EP individual events are highly correlated to their ensemble mean, with congruence coefficients around 0.3–0.7. This indicates the robust common feature in individual cases. The same conclusion is also valid for MP El Niño; most individual cases resemble the ensemble mean with spatial pattern congruence coefficients around 0.4–0.9, implying a high signal-to-noise ratio. However, in CP El Niño, the divergence among samples is slightly larger, which indicates larger uncertainty of the composite results.

b. Atmospheric circulation

Now, let us examine the relation of regional circulations over East Asia (shown in Fig. 2) with precipitation anomalies as shown in Fig. 1. It is clear that circulation anomalies differ from each other among the three types of El Niño. For EP El Niño, the wetness in the Yangtze River valley (Fig. 1b) is mainly attributed to the anomalous anticyclone over the western subtropical Pacific, obvious in Fig. 2a at 500 hPa and in Fig. 2c at 850 hPa with an anomalous center over the South China Sea. The anticyclone resembles the Philippine Sea anticyclone reported in earlier studies (Wang et al. 2003). It strengthens the western Pacific subtropical high (WPSH) and shifts its ridge line westward by 10° of longitude (as indicated by the dark red dashed line in Fig. 2a). As a result, the southwest wind at the northwest flank of the anomalous WPSH and the straight down north wind, which is associated with a weak anomalous cyclone over northeast of Lake Baikal, converge along the Yangtze River valley and lead to air ascending (Fig. 2b). In addition, at low levels, the southwesterly of the anomalous anticyclone transports abundant moisture from the South China Sea, providing a favorable water vapor condition over the Yangtze River valley (Fig. 2c). This is consistent with previous studies showing a westward shift of WPSH that can result in abundant rainfall in the Yangtze River valley (Zhang et al. 1999; Chang et al. 2000).

However, for MP El Niño, the dipolar precipitation anomaly over East Asia (Fig. 1d) is mainly ascribed to an anomalous low pressure in Northeast Asia and an anomalous anticyclone extending from the Yellow Sea to the Sea of Japan. Unlike EP, the prominent feature of MP is located at Northeast Asia. As shown in Fig. 2d, a pronounced low pressure anomaly at 500 hPa is in Northeast Asia with an east–west trough along the northeast border of China. It transports warm air (as indicated

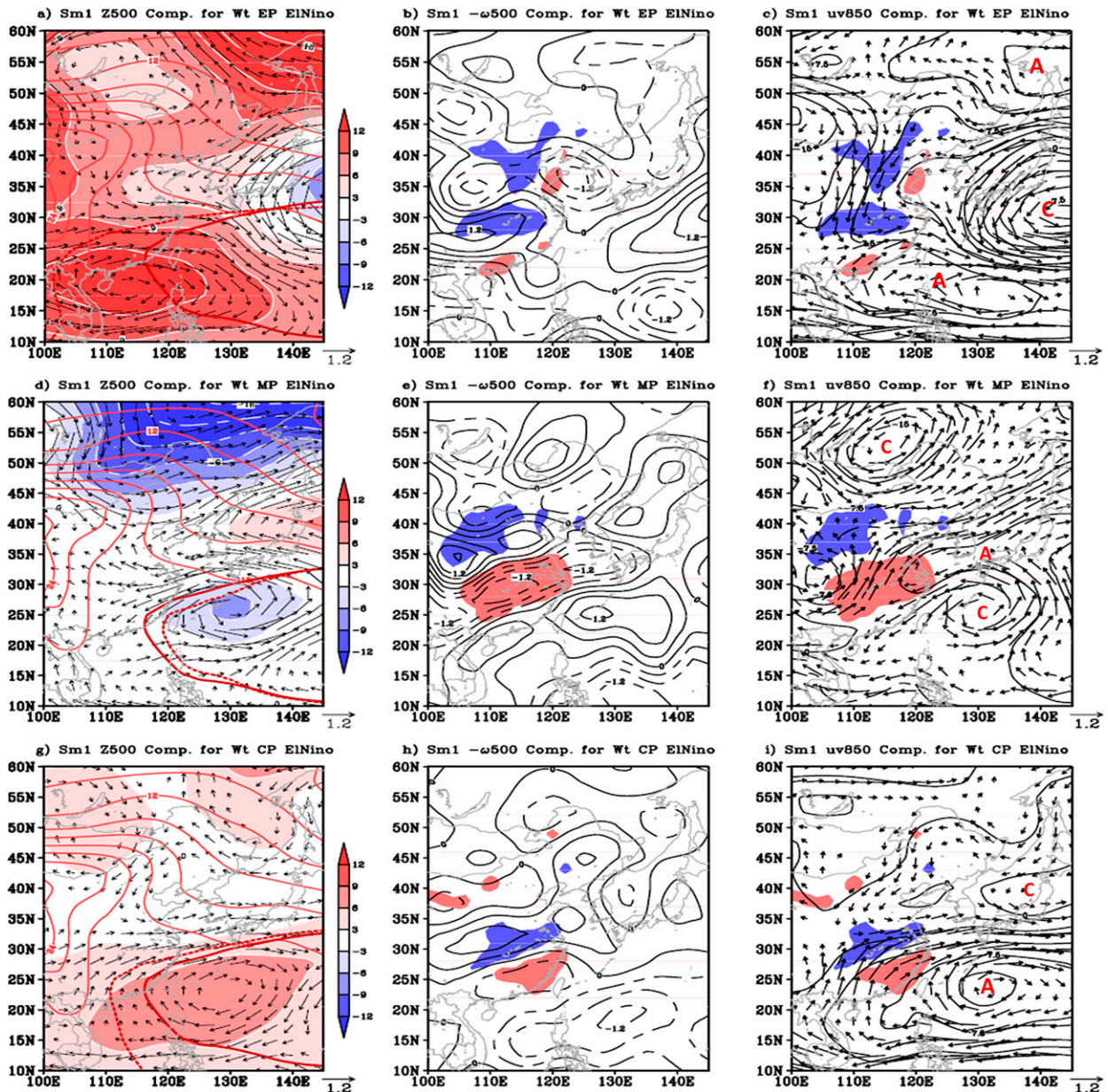


FIG. 2. Composite atmospheric anomalous fields over East Asia in El Niño decaying summer for (top) EP, (middle) MP, and (bottom) CP El Niño. (left) 500-hPa geopotential height [shading; contour interval (CI) = 3 m] and wind (vectors; unit: m s^{-1}), with 850-hPa climatological air temperature plotted in red contours (CI = 2°C). The thick red dashed (solid) contour is the 5860-m geopotential height line, which indicates the composite (climatological) western Pacific subtropical high. (center) 500-hPa vertical velocity ($-\omega$) with CI = $0.4 \times 10^{-2} \text{ Pa s}^{-1}$. (right) 850-hPa geopotential height (black contours; CI = 2.5 m) and wind (vectors; m s^{-1} ; omitted if less than 0.2 m s^{-1}). The red letters C and A mark the cyclones and anticyclones, respectively. The shading in the center and right panels from top to bottom indicate the precipitation anomalies in Figs. 1b, 1d, and 1f, respectively, with blue (red) for precipitation anomalies greater than +10% (less than -10%).

by the red contours in Fig. 2d) in front of the trough from northwest China into northeast China. This results in air ascent in north and northeast China (Fig. 2e), which is coincident with the wet conditions in Fig. 1d. In addition, to the south of the low pressure anomaly, it is a weak anticyclone over the Yellow Sea and the Sea of Japan with extension to central China. The

southwesterly wind at the northwest flank of the anticyclone transports abundant water vapor from the western Pacific to northern China, resulting in the anomalous rainfall in north China (Fig. 2f). However, in the Yangtze–Huanghuai River valley where prevails the anticyclone, there is dryness due to the anticyclone-induced subsidence (Figs. 2e,f). Overall,

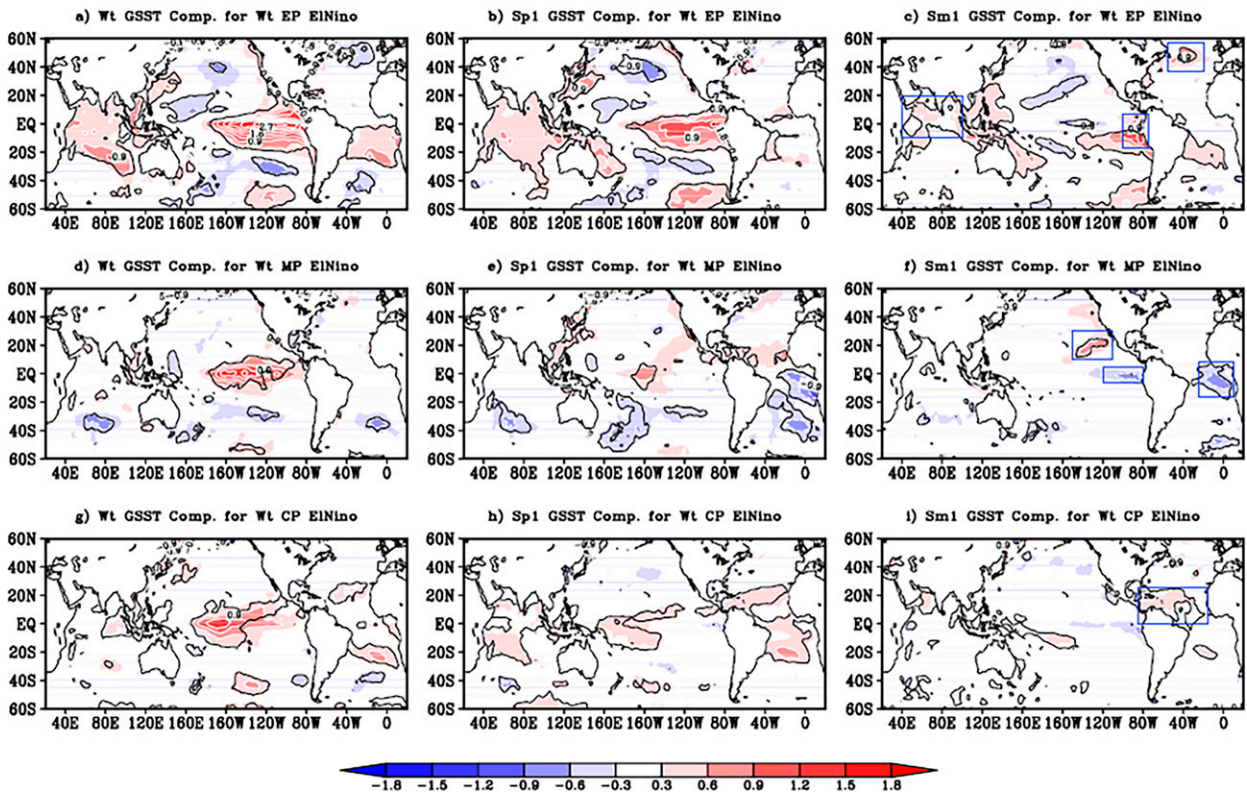


FIG. 3. Composite SST anomalies for different types of El Niño and at different stages of evolution for (top) EP, (middle) MP, and (bottom) CP El Niño. Columns show El Niño (left) mature phase of winter (DJF), (center) decaying phase of following spring (MAM), and (right) summer (JJA), respectively. The thick black contour denotes the 95% confidence level. The blue boxes at the right column indicate the key regions that relay the winter effects of EP, MP, and CP El Niño into the following summer. In (c), the regions 10°S – 20°N , 40° – 100°E ; 17°S – 7°N , 100°W – 75°W ; and 37° – 57°N , 55° – 20°W are for the TIO, tropical Pacific residual El Niño, and NA indexes, respectively. In (f), the regions are 10° – 30°N , 150° – 110°W for NSP, 6°S – 5°N , 120° – 80°W for ETP, and 16°S – 8°N , 25°W – 10°E for STA. In (i), the region 0° – 25°N , 85° – 25°W is for the NTA index.

different from previous studies emphasizing the role of PSAC in El Niño decaying summer, Figs. 2e and 2f reveal two other key circulation patterns (the anomalous low pressure in Northeast Asia and the anomalous anticyclone in the Yellow Sea and the Sea of Japan) that cause the distinguishing precipitation response to MP El Niño.

For CP El Niño, key circulation changes to produce the precipitation anomaly in Fig. 1f are the anomalous anticyclone in the western extratropical North Pacific and the anomalous cyclone in Northeast Asia. As shown in Fig. 2g, an abnormal anticyclone at 500 hPa covers the western extratropical Pacific and southern China, which strengthens the WPSH westward to southeast China (as shown by the dark red dashed contour in Fig. 2g). To its north, there is a discernible cyclone over Northeast China (Fig. 2g). They form a confrontational meridional situation over East Asia. A cold dry air mass from the north and a warm moist air mass from the south converge over the Yangtze–Huaihe River valley, and result in ascending motions and abundant rainfall there (Figs. 2h,i). Meanwhile, in southeast China, the anomalous anticyclone induces subsidence, and therefore rain deficit (Figs. 2h,i). Comparing EP and CP El Niño, we can see that their associated precipitation anomalies are both related with the dominant anticyclone

over the western subtropical Pacific. That partly explains why the PSAC is outstanding in relating El Niño with East Asian precipitation in the following summer (Wang and Zhang 2002; Wen et al. 2020).

4. Key bridging SST anomalies sustaining El Niño delayed effects

From the above analysis, we can observe significant differences for precipitation anomalies over East Asia and associated circulation anomalies for different types of El Niño. The following question that arises naturally is how different types of winter-peaked El Niño events exert their influence on East Asian precipitation in the next summer while their SST anomalies in the equatorial Pacific almost disappear. To address this issue, we need a two-step investigation: What are the intermediate SST anomalies for different types of El Niño? How do they impact the atmospheric circulation in boreal summer?

a. SST anomalies in other basins while El Niño decays in the tropical Pacific

From the evolution of global SST anomalies within El Niño's different stages (Fig. 3), the potential oceanic basins

and SST anomalies in relaying El Niño delayed effects from its peaked winter to the next summer are quite different for each of the three types of El Niño.

For EP El Niño, the key SST anomalies might be the basin-scale warming of the tropical Indian Ocean, the residual SST anomaly over the Niño-1 and -2 regions in the tropical Pacific and the warm SST over the central North Atlantic. As shown in Figs. 3a–c, in the mature winter, besides the canonical SST anomalies in the eastern tropical Pacific (Fig. 3a), the pronounced feature is the broad warm SST anomalies in the tropical Indian Ocean, a direct consequence of remote forcing from the tropical Pacific through atmospheric bridges (Klein et al. 1999). As the evolution of El Niño progresses, warm SST anomalies in the Indian Ocean are further strengthened in the following spring to reach almost the whole tropical basin (Fig. 3b). Such a situation continues until the following summer (Fig. 3c). While the tropical Indian Ocean warms up, El Niño itself in the eastern tropical Pacific gradually decays with the anomaly center shrinking toward the west coast of South America in the following spring (Fig. 3b). In the following summer, there are only a few warm anomalies in the Niño-1 and -2 regions, but slight cold SST anomalies emerge in the eastern-central equatorial Pacific (Fig. 3c). This is consistent with our understanding of the phase transition of El Niño episode through the equatorial Kelvin wave adjustment (Suarez and Schopf 1988). In addition, unexpectedly, a warm SST anomaly in the central North Atlantic gradually develops at the decaying stage of spring and largely amplifies in the following summer (Figs. 3b,c). The maximum amplitude is around 0.9°C, comparable to the remaining SST anomaly in the Niño-1 and -2 regions. The establishment of this SST anomaly may be related to the El Niño-induced North Atlantic Oscillation (NAO) anomaly (Zhang et al. 2019) and local air–sea interaction (Cayan 1992; Wen et al. 2005).

In MP El Niño, the key SST anomalies that can relay the winter El Niño effect into the following summer are probably located in the eastern basins of the tropical Pacific and the tropical Atlantic. As shown in Figs. 3d–f, the evolution of anomalous SST is quite different from the EP case. In the mature-phase winter, except the dominant warm SST anomaly in the eastern-central equatorial Pacific, MP El Niño is accompanied by few SST anomalies in other ocean basins (Fig. 3d). However, in the following spring when its own SST anomaly declines, SST anomalies in a few other ocean basins start to develop, such as the warm anomalies in the northeast subtropical Pacific and the dipolar anomalies across the equatorial Atlantic (Fig. 3e). The subtropical Pacific structure is further strengthened in the following summer (Fig. 3f), probably due to local air–sea interaction (Yuan and Yamagata 2014). The tropical Atlantic dipolar pattern, however, significantly evolves from spring to summer, and only the cold SST anomaly in the south part remains and resembles the Atlantic Niña. This may be related to the ocean dynamics, in response to the El Niño-induced easterly wind anomalies over the equatorial Atlantic (Chang et al. 2006). In addition, in the following summer, El Niño is transforming to La Niña, with cold SST anomalies developing from the west coast of South America to the eastern equatorial Pacific. That is consistent with our understanding of the rapid evolution of El Niño to La Niña (Zhou et al. 2014). Except for these SST anomalies,

there are no other anomalies in rest of the global ocean in the decaying summer of MP El Niño (Fig. 3f). Therefore, the dipole-type SST anomalies across the equator such as the warm SST in the northeast subtropical Pacific, the emerging La Niña in the eastern equatorial regions, and the Niña-like anomaly in the southern tropical Atlantic provide the possible bridges to connect the winter MP El Niño with the following summer East Asian precipitation.

For CP El Niño, the SST anomaly in the northern tropical Atlantic could serve as a bridge. As shown in Figs. 3g–i, the pronounced feature is the long-lasting SST anomaly in the northern tropical Atlantic at the decaying stage. In the mature winter, a warm SST anomaly starts to develop in the northern tropical Atlantic (Fig. 3g). The warm SST anomaly is further strengthened in the following spring and continues into the following summer, when the central tropical El Niño SST anomaly quickly declines (Figs. 3h,i). Previous studies suggested that the warm SST anomaly in the northern tropical Atlantic is induced by El Niño by two ways: the extratropical forcing through the Pacific–North American pattern (PNA) and the tropical forcing via remote Gill response (Alexander and Scott 2002; Chang et al. 2006; Jiang and Li 2019). In addition, CP El Niño can also induce the tropical Indian Ocean basin warming in the following spring, but the SST anomaly is quickly damped in the following summer. Therefore, only the northern tropical Atlantic SST anomaly may play an important role in relaying the CP El Niño influence on the East Asian precipitation.

b. Atmospheric response to the intermediate SST anomalies

From what is shown in Fig. 3, we identified a few SST anomalies that could possibly be the relevant intermediary connecting winter-peaked El Niño to East Asian precipitation in the following summer. These SST anomalies seem well placed to create the necessary forcing to initiate and sustain the delayed atmospheric responses (Fig. 4). To demonstrate this hypothesis, we performed an EFA analysis that was designed to assess atmospheric responses to SST anomalies while complex feedbacks may operate between ocean and atmosphere. We note, however, that the SST variation here may include all variability, not just that in relation to El Niño.

Since the bridging SST anomalies identified in Fig. 3 show coherent variation in different ocean basins, we can use their domain-averaged time series in the blue boxes as indices to represent the effect of the whole basin. In the EP El Niño case, three indices are relevant, involving the tropical Indian Ocean (TIO), the tropical Pacific residual El Niño, and the central North Atlantic (NA), respectively. Due to the strong covariability between the tropical Indian Ocean basin and the Pacific zone of residual El Niño, the TIO index is then used to represent effects from the two basins. For MP El Niño, key SST anomalies are represented by the northeast subtropical Pacific (NSP), the southern tropical Atlantic (STA), and the eastern tropical Pacific (ETP). For CP El Niño, the northern tropical Atlantic (NTA) is used to calculate the representative time series of SST. All indices are normalized by their standard deviation. As shown by the regression map presented in the online supplemental materials (Figs. S1 and S2, left panels),

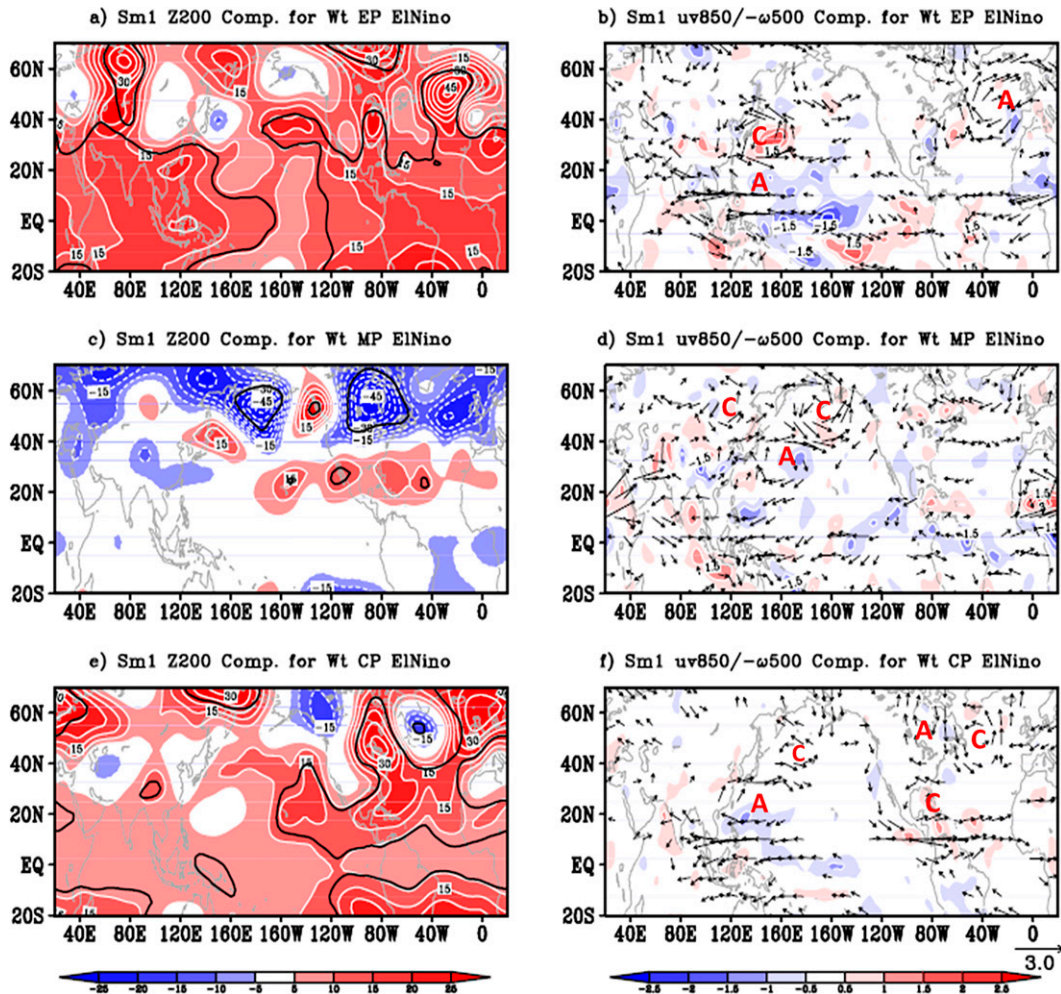


FIG. 4. Composite atmospheric anomalous fields in El Niño decaying summer for (top) EP, (middle) MP, and (bottom) CP El Niño. (left) 200-hPa geopotential height (shading; CI = 5 m), with black contours denoting the 90% confidence level. (right) 850-hPa wind (vectors; m s^{-1} ; omitted if less than 0.4 m s^{-1}) and 500-hPa vertical velocity ω with opposite sign ($-\omega$; shading, $\times 10^{-2} \text{ Pa s}^{-1}$, ascending in red and descending in blue). The red letters C and A mark cyclones and anticyclones respectively.

these index-associated SST anomalies can be well separated from each other. We can thus perform the univariate EFA analyses to assess their individual impact on atmosphere. For the sake of conciseness, we present here only their combined results to mimic the delayed effect of the three types of El Niño (Fig. 5). Atmospheric response to individual SST forcing is presented in the online supplemental material (Figs. S1 and S2, center and right panels).

To directly compare EFA results with the composite analysis, we applied different weighting factors to these SST anomalies and their individual EFA responses for the three types of El Niño (weighting factors listed in Table 2). The SST forcing and the atmospheric response are then reconstructed through a linear combination. As shown in Fig. 5 (left panels), such reconstructed SST anomalies, in the relevant key regions, are now comparable with those deduced from the composite analysis (Fig. 3, right panels).

We can now evaluate the reconstructed atmospheric circulation responses, shown in Fig. 5 (center and right panels), against their composite counterpart shown in Fig. 4. Their resemblance would confirm the role of the intermediate SST anomalies in relaying the effect of winter-peaked El Niño on the following summer's climate.

1) CASE OF EP EL NIÑO

Let us first show the global atmospheric circulation anomalies in the El Niño decaying summer, as obtained by the composite analysis (Fig. 4). In the tropics, the geopotential height at 200 hPa shows a high pressure belt. The maximum atmospheric response (around 15 m) in the tropics is located over the eastern part of the tropical Indian Ocean and the tropical Pacific. At 850 hPa (Fig. 4b), there is a broad divergent zone over the central tropical Pacific, with anomalous easterlies converging to

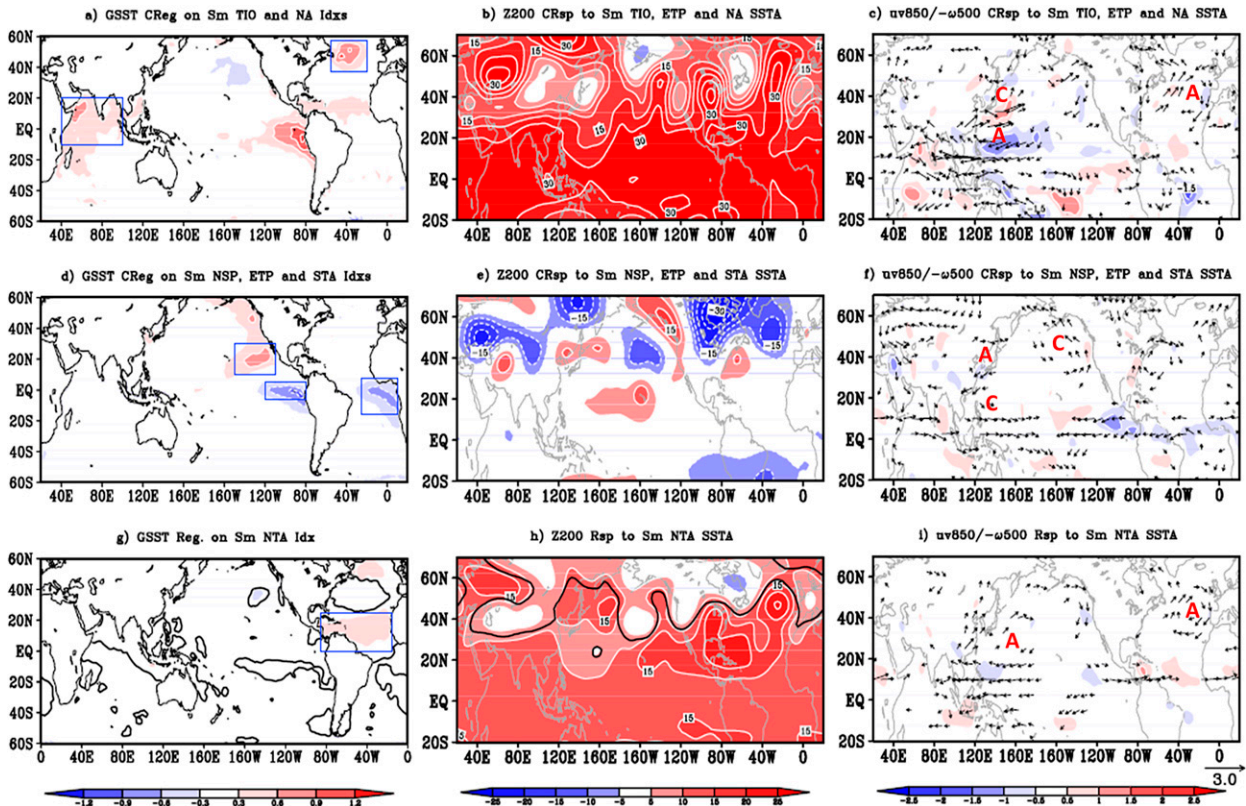


FIG. 5. (left) Reconstructed summer SST anomalies in key regions ($CI = 0.3^{\circ}C$), serving as forcings to drive the atmosphere, and (center), (right) their corresponding atmospheric responses, showing (b),(e),(h) the reconstructed responses of 200-hPa geopotential height with $CI = 5$ m and (c),(f),(i) the reconstructed responses of 850-hPa wind (vectors; unit: $m\ s^{-1}$) and 500-hPa vertical velocity ($-\omega$; shading). Results are for the (top) EP, (middle) MP, and (bottom) CP El Niño cases. Small values of wind with magnitude less than $0.4\ m\ s^{-1}$ are omitted. The red (blue) shading denotes the air ascending (descending), with $CI = 0.5 \times 10^{-2}\ Pa\ s^{-1}$. The red letters C and A mark cyclones and anticyclones respectively. The black contours in the bottom panels denote the 90% confidence level.

the tropical Indian Ocean and westerlies to the eastern tropical Pacific. Correspondingly, at 500 hPa, there is a descending zone over the central equatorial Pacific, with ascending areas on the two sides (as indicated with shading in Fig. 4b). These characteristics correspond to the SST anomaly forcings in the tropical Indian Ocean and the eastern Pacific Ocean. For middle and

TABLE 2. Weighting factors used to reconstruct atmospheric circulations from each individual EFA analysis. Their weighted combination allows to have the closest SST structures to the composite fields.

Type of El Niño	Basin-scale SST index	Weight
EP	Tropical Indian Ocean	1.8
	North Atlantic	1.1
MP	Northeast subtropical Pacific	1.0
	Eastern tropical Pacific	1.2
	Southern tropical Atlantic	0.9
CP	Tropical Atlantic	1.3

high latitudes of the Northern Hemisphere, the geopotential height at 200 hPa shows a circumglobal wave train permitting midlatitude perturbations to propagate along the zonal-wind jet. At low level, a clear meridional wave train is observed along the coast of East Asia. It shows an anomalous anticyclone over the western subtropical Pacific and an anomalous cyclone over the southeast of Japan (denoted with letters A and C, respectively, in Fig. 4b). The wave train resembles the typical Pacific–Japan (PJ) pattern in boreal summer (Kosaka and Nakamura 2010), which is stimulated with the suppressed convection over the Philippine Sea.

The above-described atmospheric circulation anomalies can be reasonably reconstructed by the EFA analysis, as shown in Fig. 5. The upper-level atmosphere presents an overall rising of geopotential height in the tropics and a circumglobal wave train in the midlatitudes (Fig. 5b), which is roughly consistent with the composite anomalies shown in Fig. 4a, the pattern congruence coefficient being 0.41. At low level, the reconstructed atmospheric response also shows strong easterlies from the western tropical Pacific to the tropical Indian Ocean, a distinguishing meridional wave train along the East Asian coast and

a robust anticyclone over the North Atlantic (Fig. 5c). The good similarity of the EFA results to the composite results constitutes a further demonstration that the intermediate SST anomalies in Fig. 3c do play an important role in sustaining the delayed effect of EP El Niño. Specifically, the SST anomalies in the tropical Indian Ocean and the eastern tropical Pacific have a major contribution to the tropical circulation anomalies, while the central North Atlantic mainly contributes to anomalies at midlatitudes (as indicated in Fig. S1). Nevertheless, we also noticed some differences between them, such as a slight westward shift of the reconstructed anticyclone over the Ural Mountains. This may be related to an eventual interference from other oceanic basins (e.g., the warm SST in the northern tropical Atlantic).

2) CASE OF MP EL NIÑO

For MP El Niño, the prominent feature of the composite circulation is the subtropical high pressure belt at 200 hPa (Fig. 4c) extending from the northeast Pacific to North Atlantic and the strong zonal wave train in midlatitudes. There are however few signals in the tropics at 200 hPa. At 850 hPa (Fig. 4d), there is a zone of divergence over the eastern equatorial Pacific and the tropical Atlantic, but a convergence zone is observed over the equatorial Indo-Pacific region. This looks like a response to the cold SST anomalies in the eastern equatorial Pacific and Atlantic. At mid- to high latitudes, the atmosphere presents a barotropic low pressure belt wave train response (Fig. 4c). Significant signals occur over East Asia with an anomalous anticyclone over the western North Pacific and anomalous cyclones over Northeast Asia and the North Pacific at 850 hPa (denoted by letters A and C in Fig. 4d).

The EFA-reconstructed atmospheric response (Fig. 5) reproduces the main characteristics of the composite anomalies, although each atmospheric response to the individual SST anomaly forcing, as shown in Fig. S2, seems quite different from the composite result. At upper level, the reconstructed response shows anomalous high pressure over the eastern-central subtropical Pacific (Fig. 5e), which captures the westernmost anomaly center of the high pressure belt in Fig. 4c. Also, the reconstructed anomalous circulations in mid- to high latitudes roughly match those in the composite result (Fig. 4c). The high similarity between Figs. 5e and 4c with congruence coefficient of 0.64 indicates that the dipolar pattern SST anomalies across the equator of the eastern Pacific and the Atlantic do play an important role in relaying the winter MP El Niño influence into the following summer. Nevertheless, the atmospheric heating seems weaker in Fig. 5f, compared to the composite in Fig. 4d. The descending zones at the equator and in its south are well reproduced in Fig. 5f, but the ascending zone north of the equator is missing. This might partly explain the discrepancies found in the reconstructed response, such as the absence of a high pressure belt over the subtropical Pacific–Atlantic in the upper level and the circulation discrepancy over the western tropical Pacific in the low level.

3) CASE OF CP EL NIÑO

The composite atmospheric circulation anomalies in CP El Niño at upper levels (Fig. 4e) exhibit high pressure anomalies

over the entire tropics and a wave train at the mid- to high latitudes. The maximum high pressure anomalies at 200 hPa are located on the edge of the subtropical eastern Pacific and over the western Atlantic, closely connected with the mid- to high-latitude wave train over the North Atlantic sector. Such a configuration might be related with the heating over the northern tropical Atlantic, quite obvious in Fig. 4f with converging winds at 850 hPa and ascending motions at 500 hPa. It is well known that the subtropical North Atlantic is a privileged area for tropical perturbations to penetrate into the subtropical jet (Ding and Wang 2005; Wen et al. 2019). The mid- to high-latitude atmosphere shows a zonal wave train response with major structures over the sectors of North America and eastern Europe (Fig. 4e). It presents an obvious barotropic structure with relevant patterns at both high and low levels (Fig. 4f). At 850 hPa, there is also a robust dipolar mode with an anticyclone over the western subtropical Pacific and a cyclone over the central North Pacific (Fig. 4f). In contrast to EP, the anticyclone of CP is northward shifted. This is consistent with the finding of Feng and Chen (2021). It shows that warm SST in the north Indian Ocean is favorable for the enhancement and southward shift of the western North Pacific anticyclone during El Niño decaying summer, while warm SST in the tropical North Atlantic tends to augment the western North Pacific anticyclone and to shift it to the north. To the south of the anticyclone, strong easterly anomalies converge to the eastern tropical Indian Ocean and result in ascending motions (Fig. 4f), which implies a possible heating source over the tropical Indian Ocean. However, some previous studies (Rong et al. 2010) indicated that the heating source over the tropical North Atlantic could also induce the anticyclone anomaly over the western tropical Pacific through the equatorial Kelvin wave.

The EFA-based atmospheric responses capture main features of the composite results. As shown in Fig. 5h, besides the general rise of the geopotential height, the maximum response is located over the northern tropical Atlantic. The corresponding low-level atmospheric response shows anomalous convergent winds over there with air ascending in the middle troposphere (Fig. 5i). In the midlatitudes, an ambiguous wave train response (Fig. 5h) roughly resembles that in Fig. 4e. In short, the entire atmospheric response in upper level is significantly correlated with the composite one in Fig. 4e, with a pattern congruence coefficient of 0.38. At low level, the atmospheric response over the western tropical Pacific is consistent with that in Fig. 4f, with a distinguishing anticyclone and strong easterlies to its south. We can conclude that the SST anomaly in the northern tropical Atlantic is the right intermediary conveying the winter CP El Niño influence into the following summer.

In addition, we specifically examine the reconstructed precipitation and its associated key circulations over East Asia for the three types of El Niño. As shown in Fig. S3, for either precipitation or circulation the reconstruction results can well capture the main characteristics of the composite ones in Fig. 2. This further demonstrates that the delayed effect of El Niño on East Asian climate is realized through the intermediate SST anomalies identified in Fig. 3.

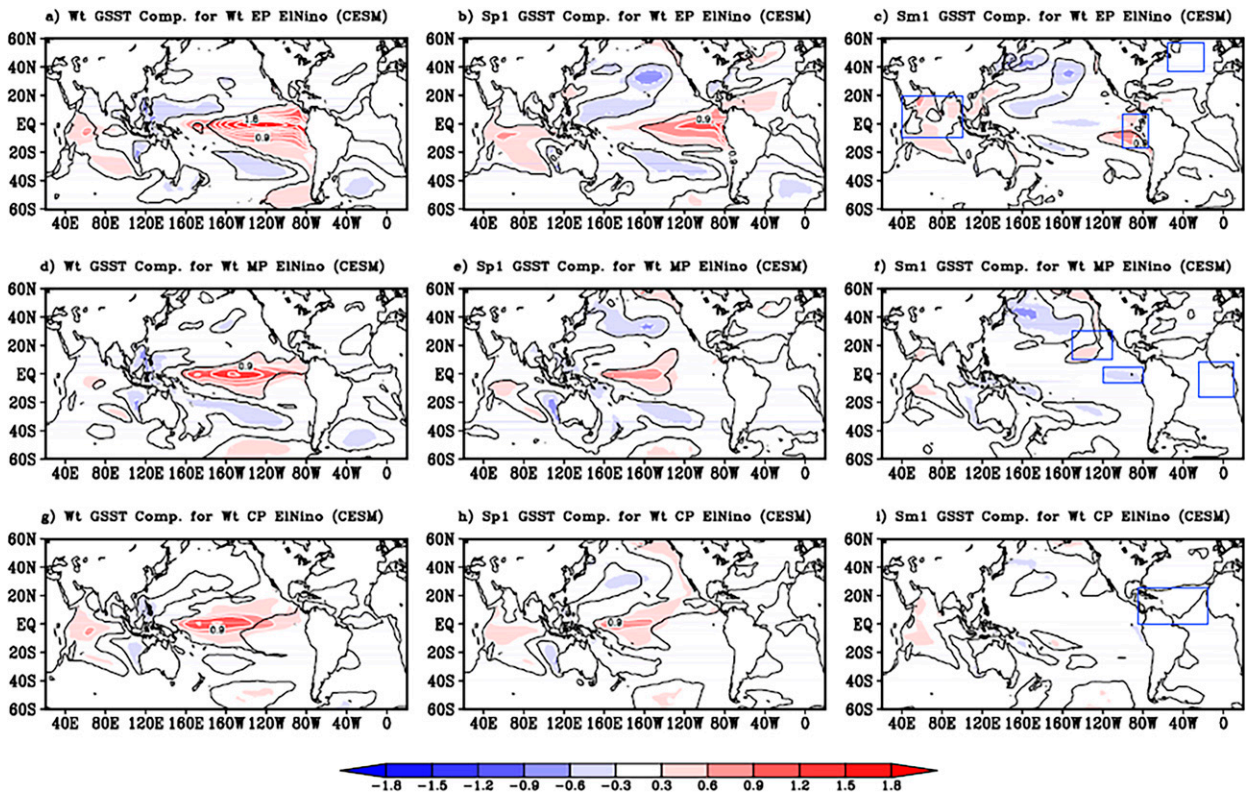


FIG. 6. As in Fig. 3, but for the Pacific pacemaker experiment (20-member ensemble average) performed with the ocean–atmosphere coupled model CESM (Deser et al. 2017). The experiment was conducted with the tropical Pacific SST maintained as observed (i.e., El Niño is the pacemaker), but the rest of the model’s global ocean is free to evolve.

c. Can the physical mechanisms be simulated in a climate system model?

We now investigate how well a climate system model can reproduce the relevant physical mechanisms that we deduced from observations alone. This issue is assessed with the Pacific pacemaker experiment (Deser et al. 2017) performed with NCAR CESM (the National Center for Atmospheric Research’s Community Earth System Model), a state-of-the-art global climate model with full ocean–atmosphere coupling. The experiment consists of maintaining the temporal evolution of the eastern tropical Pacific SST as observed through a nudging operation (10°S – 10°N in latitude, with a buffer zone extending to 20°S and 20°N , and from 180° to the American coast in longitude). The ensemble of simulations comprises 20 members covering from 1920 to 2013. We use the ensemble average and process model output in the same way as we did for observations. The global SST evolution (Fig. 6) in El Niño decaying spring and summer and the atmospheric circulation response (Fig. 7) to SST anomalies are inspected. The 2016 EP El Niño case is missing in CESM, but we believe that it does not impact our general conclusion. It is worth noting that we have also checked the GOGA (Global Ocean–Global Atmosphere) experiment of this model (atmospheric component alone, with prescribed global SST as in observation), and the simulation results can basically reproduce the observation results (as shown in Fig. S4).

Both Figs. 6 and 7 compare reasonably well with their counterpart in Figs. 3 and 4, although the signal in CESM is much weaker. The weakness of the signal is partly due to the ensemble average applied to 20 members. In fully coupled areas outside the tropical Pacific, the winter EP El Niño indeed can initiate and maintain the tropical Indian Ocean basin warming until the following summer, through atmospheric or oceanic teleconnections (as shown in Fig. 6, upper panel). But the model fails to simulate the North Atlantic SST anomaly in the following summer (Fig. 6c), although it can initiate the anomaly in the following spring (Fig. 6b). That explains why the simulated atmosphere in the following summer can only reproduce the observed characteristics in the tropics, but the feature of the midlatitude atmosphere in Fig. 4a is missing (Figs. 7a,b). For MP, winter El Niño in Fig. 6d can trigger warm SST along the west coast of North America, extended to the northeast subtropical Pacific in the following summer. The model can also simulate the observed quick transition from El Niño to La Niña (Fig. 6f). However, unlike the observation, the relation of MP El Niño with the Niña-like SST anomaly in the tropical Atlantic is too weak in the model, while the relation with the warm SST in the tropical Indian Ocean is too strong. Despite the shortcomings of the simulated SST anomalies, the atmospheric response (Fig. 7c) roughly captures the main characteristics of the composite result (Fig. 4c), with an anomalous high pressure in the subtropical Pacific and a low pressure belt in midlatitudes. In the case

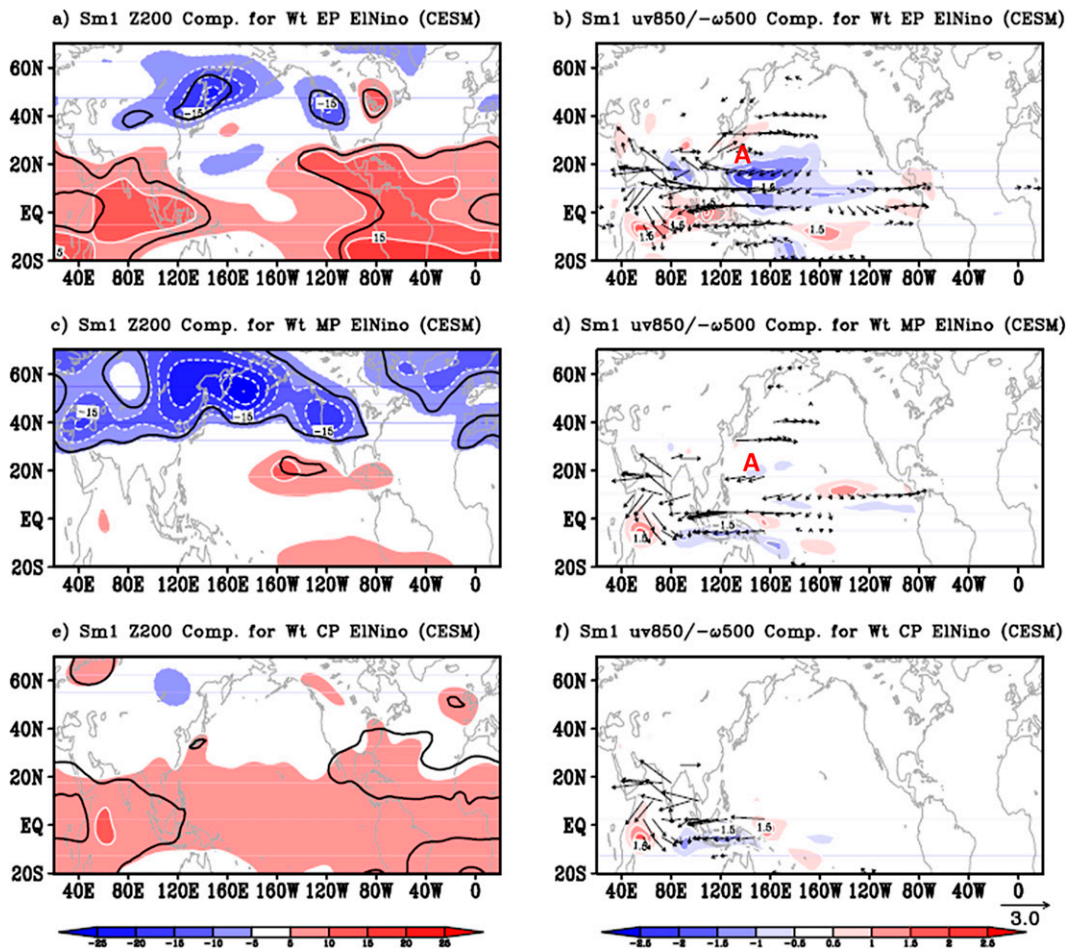


FIG. 7. As in Fig. 4, but for Pacific pacemaker experiment of CESM.

of CP El Niño, the model (Fig. 6i) still shows a strong relation of the winter El Niño with the tropical Indian Ocean in the following summer, but an ambiguous relation with the tropical Atlantic. Therefore, the simulated atmosphere (Fig. 7e) mainly presents a weak high pressure belt in the tropics, but the observed maximum value over the Atlantic sector is absent. In short, although there are some discrepancies of the simulated SST anomalies, CESM can reproduce main characteristics of the observed intermediate SST anomalies and atmospheric responses. This corroborating result enhances our confidence for the physical mechanisms that we proposed above.

5. Summary and discussion

This paper was devoted to the impacts of El Niño on East Asian precipitation in the following summer after El Niño peaks in precedent winter. Actually, this issue is highly dependent on El Niño peak-time characteristics. In our work, El Niño events are regrouped into three types: eastern Pacific (EP) El Niño, mixed-type Pacific (MP) El Niño, and central Pacific (CP) El Niño, according to the geographic locations where maximum SST anomalies occur. Our result indicates that precipitation

anomalies are significantly different for different types of El Niño and can be summarized by the schematic presented in Fig. 8. For EP El Niño, the remarkable feature is the excessive rainfall in the Yangtze River valley, which is mainly attributed to the anomalous anticyclone over the western subtropical Pacific. For MP El Niño, the precipitation shows a dipolar pattern with wet conditions in northern China and dry conditions in east-central China. This is due to the anomalous cyclone over northeast Asia and the anticyclone over the East China Sea and the Sea of Japan, providing favorable conditions for water vapor convergence and air ascending. For CP El Niño, there is a dipolar response with distinct wetness along the Yangtze–Huaihe River valley and deficient rainfall in Southeast China. It is ascribed to two key regional circulations: a cyclone in Northeast China and an anticyclone over the western tropical Pacific, forming a confrontational situation and resulting in water vapor convergence and rainfall in the Yangtze–Huaihe River valley.

The distinct precipitation response to the three types of El Niño helps us to conciliate the controversy appearing in previous studies. The abnormal dryness in the Yangtze–Huaihe Valleys in the following summer of El Niño [found in Huang and Wu

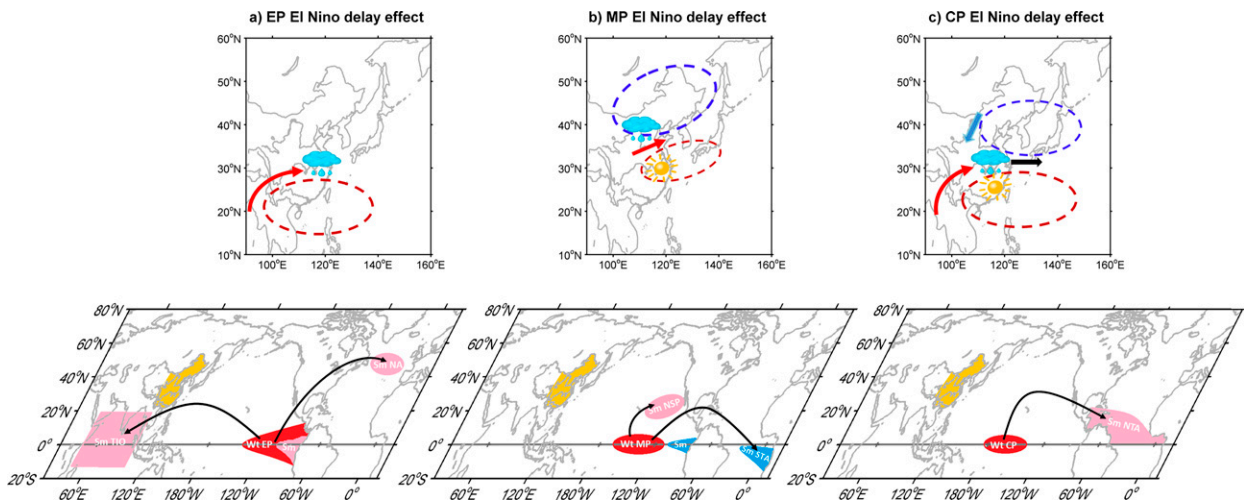


FIG. 8. Schematic showing different types of winter El Niño impacts on the following summer East Asian precipitation through their associated intermediate SST anomalies. (a) EP El Niño. Excessive rainfall along the Yangtze River valley and its associated key circulation of the anomalous anticyclone over the western subtropical Pacific (dark red dashed oval) are mainly caused by the winter EP El Niño–induced basin warming of the tropical Indian Ocean, the residual SST anomaly over the Niño-1 and -2 regions, and the warm SST over the central North Atlantic in the following summer (pink shading). (b) MP El Niño. Precipitation anomalies show a dipolar pattern with dry conditions in the Jianghuai region and wet conditions in northern and northeastern China, which is mainly attributed to the anomalous cyclone over Northeast Asia (blue dashed oval) and the weak anomalous anticyclone over east-central China (dark red dashed circle). These precipitation and circulation anomalies are fundamentally caused by the MP El Niño’s intermediate SST anomalies in the following summer, such as the warm SST in the northeast subtropical Pacific (pink shading), the emerging La Niña in the eastern equatorial Pacific and La Niña-like anomaly in the southern tropical Atlantic (blue shading). (c) CP El Niño. Precipitation anomalies show wetness in the Yangtze–Huaihe River valley and dryness in southeast China, due to the weak low pressure over North China (blue dashed oval) and the westward shifted western Pacific subtropical high (dark red dashed circle). They are mainly caused by the winter CP El Niño–induced warm SST anomaly over the northern tropical Atlantic in the following summer (pink shading). (top) Red and blue arrows indicate warm and cold advections. (bottom) Red shading indicates the different types of winter El Niño, and the yellow shading denotes the target area of this study.

(1989), Chen (2002), and Wu et al. (2003)] mainly reflects the precipitation characteristics of MP El Niño, while wetness found in the decaying summer of super El Niño events (Zhang et al. 1999; Wang and Zhang 2002; Wu et al. 2009) mainly captures the precipitation characteristics of EP El Niño. If precipitation response was assessed with the single winter Niño-3.4 index, the corresponding results would include competing effects from the three distinct types of El Niño. As shown in Wen and Hao (2021, their Fig. 3d), the broad wetness over northern China and dryness along the East Asian coast mainly reflect the MP El Niño influence, due to the weak precipitation response over north China in EP and CP El Niño cases. But their excessive rainfalls over the middle reaches of the Yangtze River are mainly associated with EP and CP El Niños. We believe that our clustering of El Niño events into three types is more relevant than what reported in previous studies using only two types (EP and CP). Because, the out-of-phase precipitation response, for MP El Niño, over the plain between the Yangtze River and the Huaihe River in East China, can eliminate the signal of precipitation whatever it is mixed into EP or CP El Niño.

Besides East Asian precipitation, large-scale atmospheric circulation, especially in the upper level, also differs significantly for the three types of El Niño. The distinct East Asian precipitation and atmospheric responses are essentially attributed to the different SST anomalies in El Niño decaying summer (as

shown by the schematic Fig. 8). For EP El Niño, the basin-scale warming of the tropical Indian Ocean, combined with the residual SST anomalies in the Niño-1 and -2 regions and the warm SST anomalies in the central North Atlantic, conveys the winter EP El Niño influence into the following summer. In the case of MP El Niño, the key bridging SST anomalies are the warm SST anomaly in the northeast subtropical Pacific, the developing La Niña in the eastern tropical Pacific and the cold SST anomaly in the southern tropical Atlantic. However, for CP El Niño, the warm SST anomaly in the northern tropical Atlantic plays an important role in relaying the winter El Niño effect. The intermediate role of such SST anomalies from other basins while El Niño decays is further confirmed using equilibrium feedback assessment (EFA) analysis. It allows us to conclude that atmospheric responses to these intermediate SST anomalies can well reproduce the main characteristics for each type of El Niño. Numerical simulations, performed with the eastern tropical Pacific El Niño signal imposed as a pacemaker in the global ocean–atmosphere coupled model CESM, basically confirm our conclusion for the role of intermediate SST anomalies in the delayed effects of different types of El Niño.

From our analysis, we can see the intermediate SST anomalies that relay El Niño’s delayed effect into the following summer are more complicated than what we thought before (Zhou et al. 2014; Xie et al. 2016; Li et al. 2017). Besides the capacitor effect

from the tropical Indian Ocean (Xie et al. 2009) or the tropical Atlantic (Rong et al. 2010), there are also joint effects of SST anomalies from other ocean basins for EP and MP El Niño. Especially for MP El Niño, the intermediate SST anomalies revealed here have never been noticed before. These SST anomalies need more investigation to understand their bridging role in El Niño delayed effect in the future. In particular, properly designed numerical simulations would help us to elucidate the physical mechanisms behind their role of intermediary to relay the effects of El Niño.

There are also other issues that we need to pursue in our future work. For example, what are the specific physical processes in the formation of these key SST anomalies and in their evolution from El Niño–peaked winter to the following summer? Why can the EP El Niño–induced SST anomaly in the tropical Indian Ocean last until the following summer, while the other two types cannot? Similarly, why is the MP El Niño associated with the Atlantic Niña in the following summer, while the CP El Niño is closely associated with the warm SST anomaly in the northern tropical Atlantic? All these questions deserve further investigation.

Acknowledgments. This work is supported by the Natural Science Foundation of China (NSFC41475089) and National Key R&D Program of China (2020YFA0608901). We thank Prof. Zhengyu Liu for many useful discussions. We are also grateful for the editor and anonymous reviewers for their constructive comments. We acknowledge the NCAR CESM Climate Variability and Change Working Group for performing and making freely available the simulations (https://www.cesm.ucar.edu/working_groups/CVC) presented in section 4c.

REFERENCES

- Alexander, M., and J. Scott, 2002: The influence of ENSO on air–sea interaction in the Atlantic. *J. Geophys. Res. Lett.*, **29**, 1701, <https://doi.org/10.1029/2001GL014347>.
- Ashok, K., S. K. Behera, S. A. Rao, H. Weng, and T. Yamagata, 2007: El Niño Modoki and its possible teleconnection. *J. Geophys. Res.*, **112**, C11007, <https://doi.org/10.1029/2006JC003798>.
- Cayan, D. R., 1992: Latent and sensible heat flux anomalies over the northern oceans: Driving the sea surface temperature. *J. Phys. Oceanogr.*, **22**, 859–881, [https://doi.org/10.1175/1520-0485\(1992\)022<0859:LASHFA>2.0.CO;2](https://doi.org/10.1175/1520-0485(1992)022<0859:LASHFA>2.0.CO;2).
- Chang, C. P., Y. Zhang, and T. Li, 2000: Interannual and interdecadal variations of the East Asian summer monsoon and tropical Pacific SSTs. Part II: Meridional structure of the monsoon. *J. Climate*, **13**, 4326–4340, [https://doi.org/10.1175/1520-0442\(2000\)013<4326:IAIVOT>2.0.CO;2](https://doi.org/10.1175/1520-0442(2000)013<4326:IAIVOT>2.0.CO;2).
- Chang, P., Y. Fang, R. Saravanan, L. Ji, and H. Seidel, 2006: The cause of the fragile relationship between the Pacific El Niño and the Atlantic Niño. *Nature*, **443**, 324–328, <https://doi.org/10.1038/nature05053>.
- Chen, W., 2002: Impacts of El Niño and La Niña on the cycle of East Asian winter and summer monsoon (in Chinese). *Chin. J. Atmos. Sci.*, **26**, 595–610, <https://doi.org/10.3878/j.issn.1006-9895.2002.05.02>.
- Chen, Z., Z. Wen, R. Wu, X. Lin, and J. Wang, 2016: Relative importance of tropical SST anomalies in maintaining the western North Pacific anomalous anticyclone during El Niño to La Niña transition years. *Climate Dyn.*, **46**, 1027–1041, <https://doi.org/10.1007/s00382-015-2630-1>.
- Dee, R. P., and Coauthors, 2011: The ERA-Interim reanalysis: Configuration and performance of the data assimilation system. *Quart. J. Roy. Meteor. Soc.*, **137**, 553–597, <https://doi.org/10.1002/qj.828>.
- Deser, C., I. R. Simpson, K. A. McKinnon, and A. S. Phillips, 2017: The Northern Hemisphere extratropical atmospheric circulation response to ENSO: How well do we know it and how do we evaluate models accordingly? *J. Climate*, **30**, 5059–5082, <https://doi.org/10.1175/JCLI-D-16-0844.1>.
- Ding, Q., and B. Wang, 2005: Circumglobal teleconnection in the Northern Hemisphere summer. *J. Climate*, **18**, 3483–3505, <https://doi.org/10.1175/JCLI3473.1>.
- Feng, J., and W. Chen, 2021: Roles of the North Indian Ocean SST and tropical North Atlantic SST in the latitudinal extension of the anomalous western North Pacific anticyclone during the El Niño decaying summer. *J. Climate*, **34**, 8503–8517, <https://doi.org/10.1175/JCLI-D-20-0802.1>.
- , —, C.-Y. Tam, and W. Zhou, 2011: Different impacts of El Niño and El Niño Modoki on China rainfall in the decaying phases. *Int. J. Climatol.*, **31**, 2091–2101, <https://doi.org/10.1002/joc.2217>.
- , —, and X. C. Wang, 2020: Re-intensification of the anomalous western North Pacific anticyclone during the El Niño Modoki decaying summer: Relative importance of tropical Atlantic and Pacific SST anomalies. *J. Climate*, **33**, 3271–3288, <https://doi.org/10.1175/JCLI-D-19-0154.1>.
- Frankignoul, C., A. Czaja, and B. L’Heveder, 1998: Air–sea feedback in the North Atlantic and surface boundary conditions for ocean models. *J. Climate*, **11**, 2310–2324, [https://doi.org/10.1175/1520-0442\(1998\)011<2310:ASFITN>2.0.CO;2](https://doi.org/10.1175/1520-0442(1998)011<2310:ASFITN>2.0.CO;2).
- He, C., T. Zhou, and B. Wu, 2015: The key oceanic regions responsible for the interannual variability of the western North Pacific subtropical high and associated mechanisms. *J. Meteor. Res.*, **29**, 562–575, <https://doi.org/10.1007/s13351-015-5037-3>.
- Hong, C.-C., T.-C. Chang, and H.-H. Hsu, 2014: Enhanced relationship between the tropical Atlantic SST and the summertime western North Pacific subtropical high after the early 1980s. *J. Geophys. Res. Atmos.*, **119**, 3715–3722, <https://doi.org/10.1002/2013JD021394>.
- Hoskins, B. J., and D. J. Karoly, 1981: The steady linear response of a spherical atmosphere to thermal and orographic forcing. *J. Atmos. Sci.*, **38**, 1179–1196, [https://doi.org/10.1175/1520-0469\(1981\)038<1179:TSLROA>2.0.CO;2](https://doi.org/10.1175/1520-0469(1981)038<1179:TSLROA>2.0.CO;2).
- Huang, R., and Y. Wu, 1989: The influence of ENSO on the summer climate change in China and its mechanism. *Adv. Atmos. Sci.*, **6**, 1179–1196, <https://doi.org/10.1007/BF02656915>.
- Jiang, L., and T. Li, 2019: Relative roles of El Niño-induced extratropical and tropical forcing in generating tropical North Atlantic (TNA) SST anomaly. *Climate Dyn.*, **53**, 3791–3804, <https://doi.org/10.1007/s00382-019-04748-7>.
- Kalnay, E., and Coauthors, 1996: The NCEP/NCAR 40-Year Reanalysis Project. *Bull. Amer. Meteor. Soc.*, **77**, 437–471, [https://doi.org/10.1175/1520-0477\(1996\)077<0437:TNYRP>2.0.CO;2](https://doi.org/10.1175/1520-0477(1996)077<0437:TNYRP>2.0.CO;2).
- Kao, H. Y., and J. Y. Yu, 2009: Contrasting eastern-Pacific and central-Pacific types of ENSO. *J. Climate*, **22**, 615–632, <https://doi.org/10.1175/2008JCLI2309.1>.
- Karori, M. A., J. P. Li, and F.-F. Jin, 2013: The asymmetric influence of the two types of El Niño and La Niña on summer rainfall over southeast China. *J. Climate*, **26**, 4567–4582, <https://doi.org/10.1175/JCLI-D-12-00324.1>.

- Klein, S. A., B. J. Soden, and N.-C. Lau, 1999: Remote sea surface temperature variations during ENSO: Evidence for a tropical atmospheric bridge. *J. Climate*, **12**, 917–932, [https://doi.org/10.1175/1520-0442\(1999\)012<0917:RSSTVD>2.0.CO;2](https://doi.org/10.1175/1520-0442(1999)012<0917:RSSTVD>2.0.CO;2).
- Kosaka, Y., and H. Nakamura, 2010: Mechanisms of meridional teleconnection observed between a summer monsoon system and a subtropical anticyclone. Part I: The Pacific–Japan pattern. *J. Climate*, **23**, 5085–5108, <https://doi.org/10.1175/2010JCLI3413.1>.
- Kug, J.-S., F.-F. Jin, and S.-I. An, 2009: Two types of El Niño events: Cold tongue El Niño and warm pool El Niño. *J. Climate*, **22**, 1499–1515, <https://doi.org/10.1175/2008JCLI2624.1>.
- Li, T., B. Wang, B. Wu, T. Zhou, C. P. Chang, and R. Zhang, 2017: Theories on formation of an anomalous anticyclone in western North Pacific during El Niño: A review. *J. Meteor. Res.*, **31**, 987–1006, <https://doi.org/10.1007/s13351-017-7147-6>.
- Li, X., W. Zhou, D. Chen, C. Y. Li, and C. Song, 2014: Water vapor transport and moisture budget over eastern China: Remote forcing from the two types of El Niño. *J. Climate*, **27**, 8778–8792, <https://doi.org/10.1175/JCLI-D-14-00049.1>.
- Li, Z. X., and S. Conil, 2003: Transient response of an atmospheric GCM to North Atlantic SST anomalies. *J. Climate*, **16**, 3993–3998, [https://doi.org/10.1175/1520-0442\(2003\)016<3993:TROAAG>2.0.CO;2](https://doi.org/10.1175/1520-0442(2003)016<3993:TROAAG>2.0.CO;2).
- Liu, Z., N. Wen, and Y. Liu, 2008: On the assessment of non-local climate feedback: I: The generalized equilibrium feedback analysis. *J. Climate*, **21**, 134–148, <https://doi.org/10.1175/2007JCLI1826.1>.
- Pascolini-Campbell, M., D. Zanchettin, O. Bothe, C. Timmreck, D. Matei, J. H. Jungclaus, and H.-F. Graf, 2014: Toward a record of central Pacific El Niño events since 1880. *Theor. Appl. Climatol.*, **119**, 379–389, <https://doi.org/10.1007/s00704-014-1114-2>.
- Peng, S., and J. S. Whitaker, 1999: Mechanisms determining the atmospheric response to midlatitude SST anomalies. *J. Climate*, **12**, 1393–1408, [https://doi.org/10.1175/1520-0442\(1999\)012<1393:MDTART>2.0.CO;2](https://doi.org/10.1175/1520-0442(1999)012<1393:MDTART>2.0.CO;2).
- Rasmusson, E. M., and T. H. Carpenter, 1982: Variations in tropical sea surface temperature and surface wind fields associated with the Southern Oscillation/El Niño. *Mon. Wea. Rev.*, **110**, 354–384, [https://doi.org/10.1175/1520-0493\(1982\)110<0354:VITSST>2.0.CO;2](https://doi.org/10.1175/1520-0493(1982)110<0354:VITSST>2.0.CO;2).
- Rayner, N. A., D. E. Parker, E. B. Horton, C. K. Folland, L. V. Alexander, D. P. Rowell, E. C. Kent, and A. Kaplan, 2003: Global analyses of sea surface temperature, sea ice, and night marine air temperature since the late nineteenth century. *J. Geophys. Res.*, **108**, 4407, <https://doi.org/10.1029/2002JD002670>.
- Rong, X. Y., R. H. Zhang, and T. Li, 2010: Impacts of Atlantic sea surface temperature anomalies on Indo–East Asian summer monsoon–ENSO relationship. *Chin. Sci. Bull.*, **55**, 2458–2468, <https://doi.org/10.1007/s11434-010-3098-3>.
- Ropelewski, C. F., and M. S. Halpert, 1987: Global and regional scale precipitation patterns associated with the El Niño/Southern Oscillation. *Mon. Wea. Rev.*, **115**, 1606–1626, [https://doi.org/10.1175/1520-0493\(1987\)115<1606:GARSPP>2.0.CO;2](https://doi.org/10.1175/1520-0493(1987)115<1606:GARSPP>2.0.CO;2).
- Suarez, M., and P. Schopf, 1988: A delayed action oscillation for ENSO. *J. Atmos. Sci.*, **45**, 3283–3287, [https://doi.org/10.1175/1520-0469\(1988\)045<3283:ADAOFE>2.0.CO;2](https://doi.org/10.1175/1520-0469(1988)045<3283:ADAOFE>2.0.CO;2).
- Taschetto, A. S., and M. H. England, 2009: El Niño Modoki impacts on Australian rainfall. *J. Climate*, **22**, 3167–3174, <https://doi.org/10.1175/2008JCLI2589.1>.
- Wang, B., and Q. Zhang, 2002: Pacific–East Asian teleconnection. Part II: How the Philippine Sea anomalous anticyclone is established during El Niño development. *J. Climate*, **15**, 3252–3265, [https://doi.org/10.1175/1520-0442\(2002\)015<3252:PEATPI>2.0.CO;2](https://doi.org/10.1175/1520-0442(2002)015<3252:PEATPI>2.0.CO;2).
- , R. Wu, and T. Li, 2003: Atmosphere–warm ocean interaction and its impacts on Asian–Australian monsoon variation. *J. Climate*, **16**, 1195–1211, [https://doi.org/10.1175/1520-0442\(2003\)16<1195:AOIAII>2.0.CO;2](https://doi.org/10.1175/1520-0442(2003)16<1195:AOIAII>2.0.CO;2).
- Wang, C., and X. Wang, 2013: Classifying El Niño Modoki I and II by different impacts on rainfall in southern China and typhoon tracks. *J. Climate*, **26**, 1322–1338, <https://doi.org/10.1175/JCLI-D-12-00107.1>.
- Wang, G., and H. H. Hendon, 2007: Sensitivity of Australian rainfall to inter-El Niño variations. *J. Climate*, **20**, 4211–4226, <https://doi.org/10.1175/JCLI4228.1>.
- Wen, N., and Y. Hao, 2021: Contrasting El Niño impacts on East Asian summer monsoon precipitation between its developing and decaying stages. *Int. J. Climatol.*, **41**, 2375–2382, <https://doi.org/10.1002/joc.6964>.
- , Z. Liu, Q. Liu, and C. Frankignoul, 2005: Observations of SST, heat flux and North Atlantic Ocean–atmosphere interaction. *Geophys. Res. Lett.*, **32**, L24619, <https://doi.org/10.1029/2005GL024871>.
- , —, —, and F. Claude, 2010: Observed atmospheric responses to global SST variability modes: A unified assessment using GEFA. *J. Climate*, **23**, 1739–1759, <https://doi.org/10.1175/2009JCLI3027.1>.
- , —, and Y. Liu, 2015: Direct impact of El Niño on East Asian summer precipitation in the observation. *Climate Dyn.*, **44**, 2979–2987, <https://doi.org/10.1007/s00382-015-2605-2>.
- , —, and L. Li, 2019: Direct ENSO impact on East Asian summer precipitation in the developing summer. *Climate Dyn.*, **52**, 6799–6815, <https://doi.org/10.1007/s00382-018-4545-0>.
- , L. Li, and J. Luo, 2020: Direct impacts of different types of El Niño in developing summer on East Asian precipitation. *Climate Dyn.*, **55**, 1087–1104, <https://doi.org/10.1007/s00382-020-05315-1>.
- Weng, H. Y., S. K. Behera, and T. Yamagata, 2009: Anomalous winter climate conditions in the Pacific rim during recent El Niño Modoki and El Niño events. *Climate Dyn.*, **32**, 663–674, <https://doi.org/10.1007/s00382-008-0394-6>.
- Wu, B., T. Zhou, and T. Li, 2009: Seasonally evolving dominant interannual variability modes of East Asian climate. *J. Climate*, **22**, 2992–3005, <https://doi.org/10.1175/2008JCLI2710.1>.
- Wu, R. G., Z. Z. Hu, and B. P. Kirtman, 2003: Evolution of ENSO-related rainfall anomalies in East Asia. *J. Climate*, **16**, 3742–3758, [https://doi.org/10.1175/1520-0442\(2003\)016<3742:EOERAI>2.0.CO;2](https://doi.org/10.1175/1520-0442(2003)016<3742:EOERAI>2.0.CO;2).
- Xie, S.-P., K. Hu, J. Hafner, H. Tokinaga, Y. Du, G. Huang, and T. Sampe, 2009: Indian Ocean capacitor effect on Indo-western Pacific climate during the summer following El Niño. *J. Climate*, **22**, 730–747, <https://doi.org/10.1175/2008JCLI2544.1>.
- , K. Yu, Y. Du, K. Hu, J. S. Chowdary, and G. Huang, 2016: Indo-western Pacific Ocean capacitor and coherent climate anomalies in post-ENSO summer: A review. *Adv. Atmos. Sci.*, **33**, 411–432, <https://doi.org/10.1007/s00376-015-5192-6>.
- Yang, J., Q. Liu, S.-P. Xie, Z. Liu, and L. Wu, 2007: Impact of the Indian Ocean SST basin mode on the Asian summer monsoon. *Geophys. Res. Lett.*, **34**, L02708, <https://doi.org/10.1029/2006GL028571>.
- Yeh, S.-W., J.-S. Kug, B. Dewitte, M.-H. Kwon, B. P. Kirtman, and F.-F. Jin, 2009: El Niño in a changing climate. *Nature*, **462**, 674, <https://doi.org/10.1038/nature08546>.
- Yu, J., L. Ou, L. Chen, L. Li, M. Sun, X. Zhong, and X. Zhang, 2021: Tropical cyclone genesis over the western North Pacific

- impacted by SST anomalies from other basins while El Niño decays. *Quart. J. Roy. Meteor. Soc.*, **147**, 2580–2596, <https://doi.org/10.1002/qj.4042>.
- Yuan, C., and T. Yamagata, 2014: California Niño/Niña. *Sci. Rep.*, **4**, 4801, <https://doi.org/10.1038/srep04801>.
- Yuan, Y., and S. Yang, 2012: Impacts of different types of El Niño on the East Asian climate: Focus on ENSO cycles. *J. Climate*, **25**, 7702–7722, <https://doi.org/10.1175/JCLI-D-11-00576.1>.
- Zhang, R. H., A. Sumi, and M. Kimoto, 1999: A diagnostic study of the impact of El Niño on the precipitation in China. *Adv. Atmos. Sci.*, **16**, 229–241, <https://doi.org/10.1007/BF02973084>.
- , Q. Min, and J. Su, 2017: Impact of El Niño on atmospheric circulations over East Asia and rainfall in China: Role of the anomalous western North Pacific anticyclone. *Sci. China Earth Sci.*, **60**, 1124–1132, <https://doi.org/10.1007/s11430-016-9026-x>.
- Zhang, W., Z. Wang, M. F. Stuecker, A. G. Turner, F.-F. Jin, and X. Geng, 2019: Impact of ENSO longitudinal position on teleconnections to the NAO. *Climate Dyn.*, **52**, 257–274, <https://doi.org/10.1007/s00382-018-4135-1>.
- Zhou, T., W. Bo, and D. Lu, 2014: Advances in research of ENSO changes and the associated impacts on Asian-Pacific climate. *Asia-Pac. J. Atmos. Sci.*, **50**, 405–422, <https://doi.org/10.1007/s13143-014-0043-4>.